



City Research Online

City, University of London Institutional Repository

Citation: White, M., Read, M. G. & Sayma, A. I. (2020). Making the case for cascaded organic Rankine cycles for waste-heat recovery. *Energy*, 211, 118912. doi: 10.1016/j.energy.2020.118912

This is the published version of the paper.

This version of the publication may differ from the final published version.

Permanent repository link: <https://openaccess.city.ac.uk/id/eprint/24962/>

Link to published version: <https://doi.org/10.1016/j.energy.2020.118912>

Copyright: City Research Online aims to make research outputs of City, University of London available to a wider audience. Copyright and Moral Rights remain with the author(s) and/or copyright holders. URLs from City Research Online may be freely distributed and linked to.

Reuse: Copies of full items can be used for personal research or study, educational, or not-for-profit purposes without prior permission or charge. Provided that the authors, title and full bibliographic details are credited, a hyperlink and/or URL is given for the original metadata page and the content is not changed in any way.

City Research Online:

<http://openaccess.city.ac.uk/>

publications@city.ac.uk



Making the case for cascaded organic Rankine cycles for waste-heat recovery



Martin T. White^{*}, Matthew G. Read, Abdulnaser I. Sayma

Department of Mechanical Engineering and Aeronautics, School of Mathematics, Computer Science and Engineering, City, University of London, Northampton Square, London, EC1V 0HB, UK

ARTICLE INFO

Article history:

Received 5 February 2020
Received in revised form
18 August 2020
Accepted 20 September 2020
Available online 1 October 2020

Keywords:

Organic rankine cycle
ORC
Cascaded
Waste-heat recovery
Optimisation
Expander modelling

ABSTRACT

The design of single-stage organic Rankine cycle (ORC) systems can be challenging owing to large volumetric expansion ratios and sub-atmospheric condensation pressures. Cascaded systems could lead to more efficient expansion processes, higher condensation pressures, whilst introducing the possibility of two-phase expansion to enhance performance. The aim of this paper is to compare single-stage ORC systems to a novel two-phase cascaded system that combines a two-phase expansion topping cycle and a single-phase bottoming cycle for waste-heat recovery applications. Thermodynamic cycle models are integrated with variable efficiency expander models and discretised heat-exchanger sizing models, and single- and multi-objective optimisation studies are completed for three heat-source temperatures (473, 523 and 573 K). The results indicate the relative performance improvement of cascaded systems increases as the heat-source temperature and relative heat-sink size increase, and could increase power output and first-law thermal efficiency by up to 11.1% and 9.5% respectively. The multi-objective optimisation reveals that for a fixed total heat-transfer area the cascaded systems produce approximately 3.6% and 10.5% more power than the single-stage systems for the 523 and 573 K cases respectively with a heat-sink mass-flow rate of 1 kg/s. This increases to 11.7% and 14.5% for heat-sink mass-flow rate of 4 kg/s.

© 2020 The Author(s). Published by Elsevier Ltd. This is an open access article under the CC BY license (<http://creativecommons.org/licenses/by/4.0/>).

1. Introduction

Organic Rankine cycle (ORC) power systems are a promising technology for power generation from low-temperature heat below 400 °C, and commercial systems are available [1]. For power outputs below a few hundred kilowatts, ORC systems are typically single-stage systems constructed from a pump, evaporator, expander and condenser (Fig. 1), although a recuperator may also be included to improve the cycle thermal efficiency. The main challenges faced when designing single-stage systems arises when the heat-source temperature is at the higher end of the considered range. To maximise thermodynamic performance more molecularly complex working fluids are required, which have high normal boiling temperatures, whilst high pressure ratios are required. This leads sub-atmospheric condensation pressures, resulting in large condensers that need to operate under a vacuum, and large volumetric expansion ratios.

High volumetric expansion ratios have implications on expander selection. Radial turbines are capable of obtaining the required expansion over a single stage [2,3]. However, the large change in density across the rotor results in small rotor-inlet blade heights, introducing increased secondary flows and clearance losses [4]. Volumetric expanders may be an alternative, but are limited in volume ratio by mechanical design constraints. Thus, multiple expansion stages are required, although even then the overall expansion ratio may be limited; Read et al. [5] suggest that for a two-stage system operating with screw expanders the overall volumetric expansion ratio may be limited to 20 to achieve reasonable overall expansion efficiency. It is also worth emphasising the interest in two-phase expansion, which could increase power output from waste-heat recovery (WHR) systems [5–7]. However, the high volumetric expansion ratios required for high-temperature systems may rule out two-phase expansion, since conventional turbo-expanders are unsuitable for two-phase operation.

Cascaded systems, comprised of a high-temperature topping cycle and a low-temperature bottoming cycle (Fig. 1), could offer

^{*} Corresponding author.
E-mail address: martin.white@city.ac.uk (M.T. White).

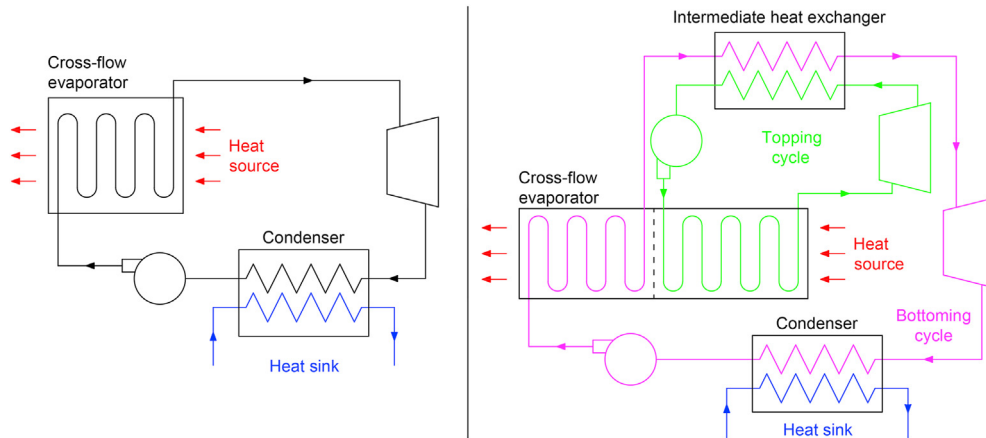


Fig. 1. Schematic of the single-stage (left) and cascaded (right) ORC systems under consideration within this study.

benefits over single-stage systems. In cascaded systems, the expansion process is effectively divided across two separate systems, and thus volumetric expansion ratios are reduced. This could result in more efficient turbines since they are not required to operate over such high expansion ratios, and introduces the possibility to use volumetric expanders and realise two-phase expansion. Moreover, one can select a fluid with a high normal boiling point for the topping cycle, and a fluid with a lower normal boiling point for the bottoming cycle, thus removing sub-atmospheric pressures. However, it should be noted that the additional complexity of the cycle may complicate start-up and shutdown procedures. Moreover, they would likely require more complex control systems to vary the operating conditions within both cycles. This is potentially an important factor that should be considered in any future techno-economic analysis.

Kane et al. [8] developed a mini-scale hybrid power plant, based on a cascaded system, that used two scroll expanders with R123 and R134a as working fluids. Their experimental results demonstrate adequate behaviour over a range of operating conditions, which confirmed system stability. However, the system was limited to temperatures below 200 °C. Cascaded systems have also been investigated for reverse osmosis desalination, where the topping cycle is used to drive the pump of the reverse osmosis unit, whilst the bottoming cycle drives the systems auxiliaries [9,10]. Rech et al. [11] studied cascaded systems for marine WHR. Their results suggest systems with a transcritical topping cycle could produce 40% more energy annually than a single-stage system. Braimakis and Karellas [12] conducted an exergetic optimisation of cascaded systems and found they only perform better within a certain range, but are a promising option when the optimal single-stage fluid is impractical due to it being unavailable or expensive. In which case, less expensive or more readily available fluids can be coupled together within a cascaded system. However, their analysis was based on fixed component efficiencies, and did not consider heat-transfer area requirements. Dubberke et al. [13] are commissioning a cascaded ORC test facility. Preliminary tests have been completed with cyclo-pentane and propane, although the results are not yet sufficient to fully evaluate the system thermodynamic performance.

Chen et al. [14] compared cascaded systems to dual-pressure systems¹ for automotive WHR, citing issues around needing two separate loops with two different working fluids as a drawback of

cascaded systems. Their results suggest dual-pressure systems could produce more power than cascaded systems, whilst requiring less heat-transfer area; although a detailed heat exchanger assessment was not completed. Manente et al. [15] investigated dual-pressure systems for heat-source temperatures ranging between 100 and 200 °C, and found that these systems can produce 20% more power than single-stage systems in certain circumstances; however, if a fluid with an optimal critical temperature ($T_{cr} = T_{hi} - 40$ °C) can be found, single-stage system may be preferential. Rashwan et al. [16] considered a dual-level system, referred to the cascaded closed loop cycle, and found this system could outperform single-stage systems for heat-source temperatures exceeding 200 °C. However, in these dual-pressure systems [14–16] only a single fluid is used and thus issues around high pressure ratios and sub-atmospheric pressures are not addressed. Moreover, no studies on cascaded systems have considered two-phase expansion, whilst dual-pressure systems may be less suitable for two-phase expansion.

Previously, the authors have undertaken preliminary comparisons of single-stage and cascaded systems for waste-heat recovery applications [17,18]. The key findings are summarised in Fig. 2, which suggest that cascaded systems could produce between 4% and 6% more power than single-stage systems for waste-heat temperatures exceeding 523 K, but require at least 20% more heat-transfer area. However, these results were obtained without considering the sensitivity of the results to the expander efficiency models used, whilst no consideration of the trade-off between power and heat-transfer area was considered. The aim of this study is to conduct a more thorough comparison with particular emphasis on comparing single-stage systems to a novel cascaded system that utilises two-phase expansion in the topping cycle, achieved via a screw expander, and a single-phase radial turbine in the bottoming cycle (2-ST). Moreover, although cascaded systems could be deployed for low heat-source temperatures, emphasis is placed on studying cascaded systems for relatively high-temperature applications where performance benefits are expected to be higher, as reported in Fig. 2, but to date have not been explored in depth. The novelty of this work lies in the integration of thermodynamic cycle analysis with variable efficiency expander models for turbine and screw expanders, heat-exchanger sizing models and multi-objective optimisation, which, to the authors' knowledge, allows a more accurate and rigorous comparison than previously conducted. Specifically, the two systems are compared in terms of power output and heat-transfer requirements under different heat-source and heat-sink conditions to establish the

¹ in a dual-pressure system a single fluid is evaporated at two different pressure levels and expanded in two separate expanders.

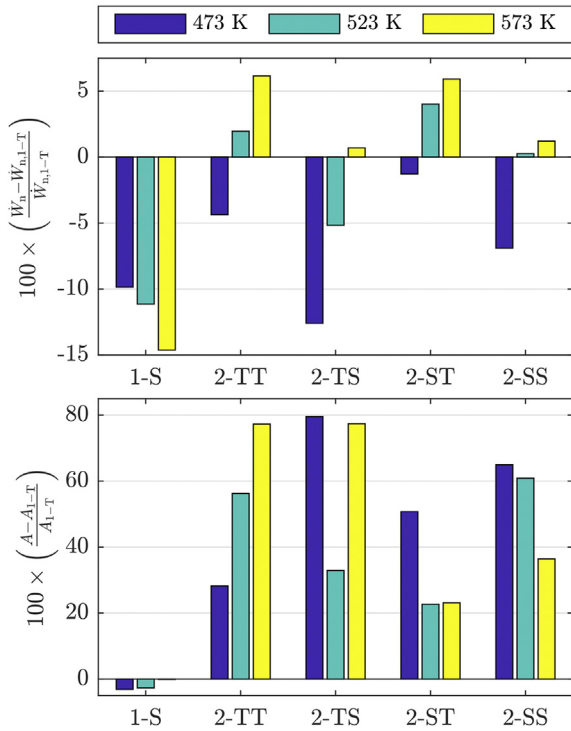


Fig. 2. Preliminary comparison of single-stage and cascaded systems for different heat-source temperatures in terms of power output \dot{W}_n (top), and total heat-transfer area A (bottom). Results are shown relative to a single-stage turbine system (1-T). 1-S refers to a single-stage screw system, and 2-TT, 2-TS, 2-ST and 2-SS refer to cascaded systems where the first and second letters denote the expander type in the topping- and bottoming cycle.

possible performance improvement achievable with the 2-ST system and whether this is at the cost of more heat-transfer area. Ultimately, these results can help establish whether there is a case for employing cascaded systems within relatively high temperature waste-heat recovery applications.

Following this introduction, the thermodynamic potential of cascaded cycles is investigated in Section 2. This is followed by a detailed description of the cascaded system model in Section 3, and a description of the case study in Section 4. The key results, including a sensitivity study concerning the expander performance models, the effect of the size of the heat sink, and results from a multi-objective optimisation study are summarised in Section 5, before the conclusions are summarised in Section 6.

2. Thermodynamic penalty of cascaded systems

To investigate the thermodynamic potential of cascaded systems a theoretical model, based on the concept of finite-time thermodynamics (FTT) [19,20], has been constructed that allows system performance to be estimated from just the heat-source and heat-sink conditions. The cascaded system is modelled as three heat engines, as shown in Fig. 3. The first represents the topping cycle, and operates between the incoming heat source, which is at a temperature T_{hi} , and an intermediate envelope, which is at a constant temperature T_{int} . The power output from this heat engine is denoted \dot{W}_t . The second represents the portion of the bottoming cycle that absorbs the remaining heat from the heat source, converts this to power (\dot{W}_{b1}), and rejects heat to the incoming heat sink, which is at a temperature T_{ci} . The third represents the second portion of the bottoming cycle that absorbs heat from the

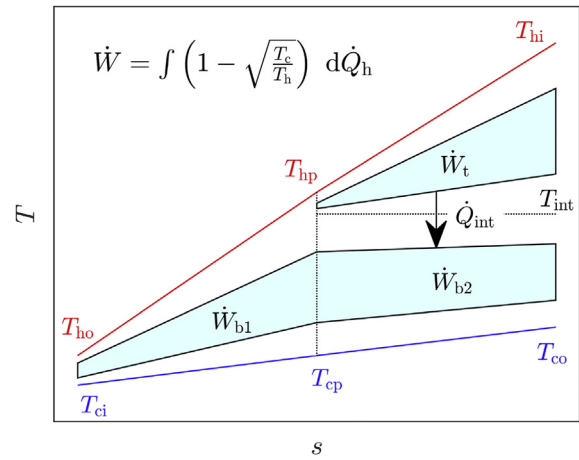


Fig. 3. Schematic of the cascaded FTT model.

intermediate envelope, converts this to power, denoted \dot{W}_{b2} , and rejects heat to the heat sink. Thus, for a given heat-source and heat-sink, both defined in terms of a temperature, mass-flow rate \dot{m} and specific-heat capacity c_p , and an assumed intermediate temperature T_{int} , the model can estimate the total power output ($\dot{W}_t + \dot{W}_{b1} + \dot{W}_{b2}$). To compare cascaded and single-stage systems, a FTT model of a single-stage system is also required. This model is identical to the one used to calculate \dot{W}_{b1} , but with the inlet heat-source temperature set to T_{hi} , rather than T_{hp} . The models are described in Appendix A.

For defined inlet temperatures (T_{hi} , T_{ci}), the performance of a cascaded system depends on T_{int} , and the ratio of the heat-sink and heat-source heat-capacity rates, defined as $\alpha = (\dot{m}c_p)_c / (\dot{m}c_p)_h$. It is also convenient to express T_{int} in the form $\theta = (T_{int} - T_{ci}) / (T_{hi} - T_{ci})$.

The findings from a comparative study between results obtained using the FTT models, and results from a cycle optimisation study, are reported in Figs. 4 and 5. The cycle models, optimisation process

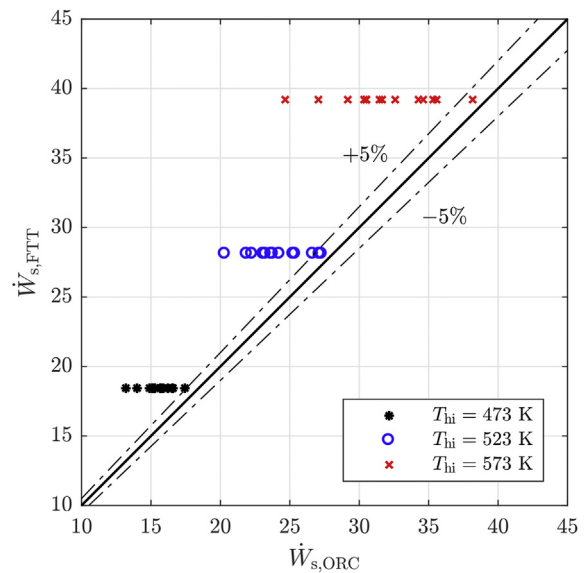


Fig. 4. Comparison between the optimal power output for a specified working fluid operating within a single-stage ORC system, $\dot{W}_{s,ORC}$, and the power predicted for a single-stage system using the FTT model, $\dot{W}_{s,FTT}$ ($T_{ci} = 288$ K, $\alpha = 4.2$).

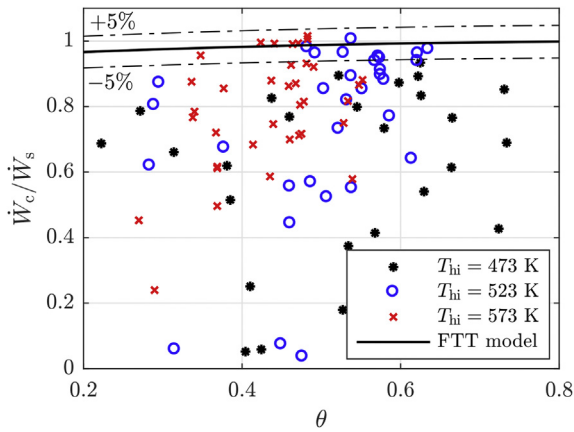


Fig. 5. Comparison between the power output from optimised cascaded systems operating with a defined pair of working fluids (markers), and results obtained using the cascaded FTT model (solid black line). Power outputs from cascaded systems, \dot{W}_c , are normalised by the power output for a single-stage system estimated using the single-stage FTT model, \dot{W}_s ($T_{ci} = 288$ K, $\alpha = 4.2$).

and assumptions are described in Section 4. For the single-stage systems (Fig. 4), the markers furthest to the right represent the optimal fluids that results in the highest power output. For the cascaded systems (Fig. 5), the markers closest to the top represent the optimal pair of working fluids that results in the highest power output. In all cases, the power outputs from the optimal cycles are within 5% of those predicted using the FTT models, providing good confidence in both FTT models.

Having established their validity, the FTT models can be used to investigate the performance of cascaded systems. The effect of α and θ on the power output are reported in Fig. 6. The top plot compares the power output from the cascaded system, \dot{W}_c , to the

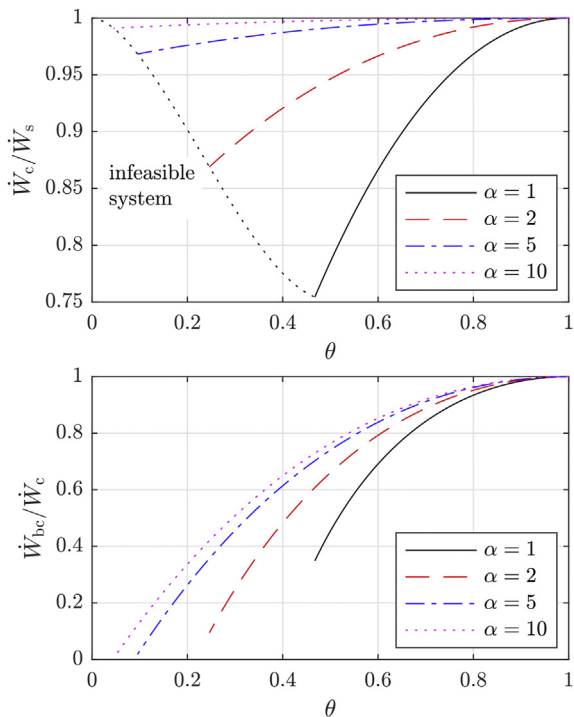


Fig. 6. Effect of θ and α on cascaded system performance relative to a single-stage system; \dot{W}_s , \dot{W}_c and \dot{W}_{bc} refer to a single-stage, full cascaded, and the bottoming-cycle of a cascaded system respectively.

power from a single-stage system operating with the same heat-source and heat-sink conditions, \dot{W}_s . The bottom plot reports the fraction of power that is generated from the bottoming cycle within cascaded systems. As T_{int} reduces, cascaded system performance degrades compared to the single-stage system (which corresponds to $\theta = 1$), and the power produced by the bottoming cycle reduces. However, as the relative size of the heat sink increases the performance degradation of the cascaded systems reduces; for $\alpha \geq 2$ and $\theta \geq 0.5$, the power reduction for the cascaded systems, relative to an optimal single-stage system, is below 5%.

Ultimately, if a single-stage system can be effectively realised (*i.e.*, an efficient single-stage expander can be obtained) this remains the optimal choice. However, if an efficient single-stage expander cannot be designed, the results in Fig. 6 suggest a cascaded system can be implemented with only a minimal degradation in performance compared to the theoretical optimum. Moreover, the best option is to maximise the temperature difference $T_{int} - T_{ci}$, which corresponds to designing the bottoming cycle with the highest volumetric expansion ratio that is possible without impeding the expander isentropic efficiency. Thus, the bottoming cycle produces most of the power, which is supplemented by a low-power topping cycle. In practical terms, this can be realised by a topping cycle operating with a volumetric expander, and a bottoming cycle operating with a turbo-expander. This allows two-phase expansion in the topping cycle, which enables a good temperature match to the heat source, whilst the isothermal intermediate heat-transfer process enables the bottoming cycle to operate with single-phase expansion using a high efficiency turbine. This minimises irreversibility, and has the advantage of compactness as the required volumetric machine is small.

3. System modelling

3.1. Thermodynamic cycle modelling

The notation used to describe the single-stage and cascaded systems is shown in Figs. 7 and 8. Both systems are assumed to operate under steady-state conditions, whilst heat losses are neglected. Fluid properties are accounted for using NIST REFPROP. The cycle analysis is completed by calculating the state points based on the input cycle variables, and applying energy balances to each heat exchanger. The pumps are modelled using a fixed isentropic efficiency, whilst the expanders are modelled according to Section 3.2. Heat-exchanger pressure drops are neglected during the cycle

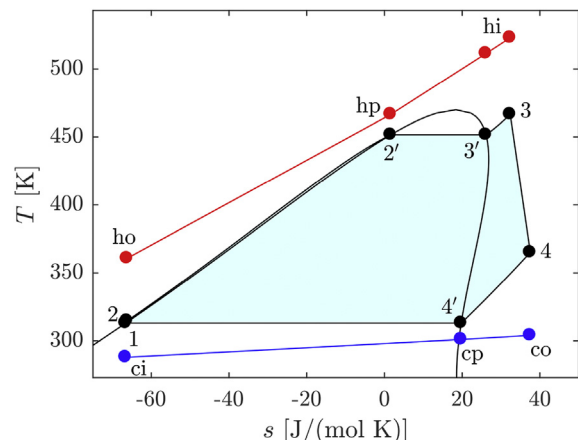


Fig. 7. $T - s$ diagram of the single-stage ORC system.

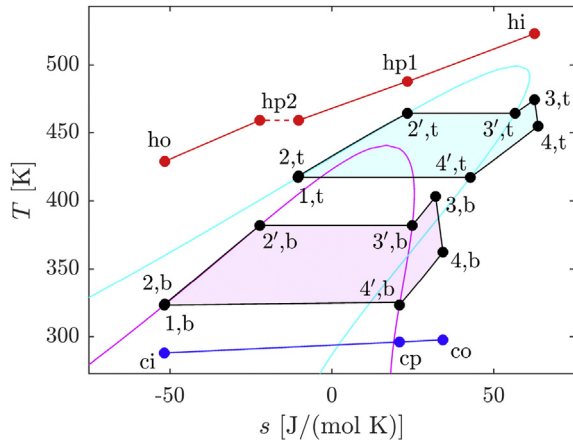


Fig. 8. $T - s$ diagram of the cascaded ORC system.

analysis, but are later evaluated during heat-exchanger sizing, and their effect on power output estimated; the validity of this approach is discussed in Section 3.3.3.

3.1.1. Single-stage ORC systems

The single-stage systems are assumed to be subcritical, non-recuperated cycles, with either single- or two-phase expansion. The analysis of this type of cycle is well documented elsewhere [21], and will not be repeated here. For this system, there are five variables that affect the power output from this system:

$$\dot{W}_n = f(T_1, p_r, PP_h, q_3, \text{fluid}), \quad (1)$$

where \dot{W}_n is the net-power output, T_1 is the condensation temperature, p_r is the reduced evaporation pressure (p_2/p_{cr} , where p_{cr} is the fluid critical pressure), and PP_h is the pinch-point temperature difference at the beginning of evaporation (i.e., $T_{hp} - T_2$). The variable q_3 defines the expander inlet conditions and allows either single- or two-phase expansion. For $q_3 \leq 1$, q_3 is equal to the expander inlet vapour quality, whilst for $q_3 > 1$, the expander inlet temperature is found from:

$$T_3 = T_{3'} + (q_3 - 1)(T_{hi} - T_{3'}), \quad (2)$$

where $T_{3'}$ is the evaporation saturation temperature and T_{hi} is the heat-source inlet temperature.

3.1.2. Cascaded ORC systems

The cascaded system is assumed to be comprised of two subcritical, non-recuperated cycles, and both cycles can operate with single- or two-phase expansion. As shown in Fig. 8, the heat source preheats, evaporates and superheats the fluid in the topping cycle, before preheating the fluid in the bottoming-cycle. The bottoming-cycle evaporation and preheating is achieved via the heat rejection from the topping cycle.

To simplify the analysis of both the single- and cascaded systems, subcooling is neglected within the thermodynamic cycle analysis and thus pumping is assumed to begin from saturated liquid conditions; although a degree of subcooling before the pump would be necessary within a practical system. However, for the optimised cycles discussed later it was found that including a subcooling of 2 K within the analysis led to relative changes in the power output and thermodynamic efficiencies that were less than 1.5% and 1.7% respectively. Thus, neglecting subcooling is not expected to have a significant effect on the optimisation results.

For the cascaded system, seven cycle variables are defined. The bottoming-cycle condensation temperature $T_{1,b}$ defines the pump inlet conditions for the bottoming cycle (i.e., $p_{1,b}$, $h_{1,b}$, $s_{1,b}$). The bottoming-cycle reduced evaporation pressure ($p_{r,b} = p_{2,b}/p_{cr,b}$) defines the evaporation temperature $T_{2,b}$, and the preheater outlet conditions (i.e., $h_{2',b}$, $s_{2',b}$), whilst the pump outlet conditions ($h_{2,b}$, $s_{2,b}$) are found from the pump efficiency. The topping-cycle condensation temperature $T_{1,t}$ is defined by the saturation temperature difference:

$$\Delta T_{\text{sat}} = T_{1,t} - T_{2',b}, \quad (3)$$

whilst the topping-cycle reduced evaporation pressure ($p_{r,t} = p_{2,t}/p_{cr,t}$) is an input. The topping-cycle pump outlet conditions ($h_{2,t}$, $s_{2,t}$) are calculated using the pump isentropic efficiency.

The topping-cycle expander inlet conditions are defined from $q_{3,t}$, which allows both single- and two-phase expansion. Thus, if $q_{3,t} < 1$, $q_{3,t}$ is equal to the topping-cycle expander inlet vapour quality, whilst for $q_{3,t} > 1$ the expander inlet temperature is found from:

$$T_{3,t} = T_{3',t} + (q_{3,t} - 1)(T_{hi} - T_{3',t}), \quad (4)$$

where $T_{3',t}$ is the topping-cycle evaporation saturation temperature and T_{hi} is the heat-source inlet temperature. The expander outlet conditions ($h_{4,t}$, $s_{4,t}$) are determined using the appropriate expander model (see Section 3.2).

The topping-cycle mass-flow rate \dot{m}_t is found by applying an energy balance to the evaporator:

$$\dot{m}_t = \frac{\dot{m}_h c_{p,h} (T_{hi} - T_{hp1})}{h_{3,t} - h_{2',t}}, \quad (5)$$

where \dot{m}_h and $c_{p,h}$ are the heat-source mass-flow rate and specific-heat capacity respectively, and T_{hp1} is the heat-source temperature at the start of evaporation in the topping cycle, and is defined by the input pinch-point temperature difference:

$$PP_h = T_{hp1} - T_{2',t}. \quad (6)$$

The bottoming-cycle mass-flow rate \dot{m}_b is found from an energy balance of the bottoming-cycle preheater:

$$\dot{m}_b = \frac{\dot{m}_h c_{p,h} (T_{hp2} - T_{ho})}{h_{2',b} - h_{2,b}}, \quad (7)$$

where T_{ho} is the heat-source outlet temperature, which is final cycle variable, and T_{hp2} is the heat-source temperature at the outlet of the topping-cycle preheater, which is found by applying an energy balance to the topping-cycle preheater:

$$T_{hp2} = T_{hp1} - \frac{\dot{m}_t (h_{2',t} - h_{2,t})}{\dot{m}_h c_{p,h}}. \quad (8)$$

The bottoming-cycle expander inlet conditions are found from an energy balance of the intermediate heat-transfer process:

$$h_{3,b} = h_{2',b} + \frac{\dot{m}_t (h_{4,t} - h_{1,t})}{\dot{m}_b}, \quad (9)$$

and the expander outlet conditions ($h_{4,b}$, $s_{4,b}$) are determined using the appropriate expander model.

A final energy balance is applied to the bottoming-cycle

condenser to determine the heat-sink outlet temperature:

$$T_{co} = T_{ci} + \frac{\dot{m}_b (h_{4,b} - h_{1,b})}{\dot{m}_c c_{p,c}}, \quad (10)$$

where T_{ci} is the heat-sink temperature and \dot{m}_c and $c_{p,c}$ are the heat-sink mass-flow rate and specific-heat capacity respectively. The condenser pinch point is also calculated and a constraint is applied during optimisation to ensure this is not below a minimum allowable value.

The thermodynamic performance of the cycle is evaluated from the net power output:

$$\dot{W}_n = \dot{W}_{n,t} + \dot{W}_{n,b} = \dot{m}_t [(h_{3,t} - h_{4,t}) - (h_{2,t} - h_{1,t})] + \dot{m}_b [(h_{3,b} - h_{4,b}) - (h_{2,b} - h_{1,b})]. \quad (11)$$

which is a function of nine variables:

$$\dot{W}_n = f(T_{1,b}, p_{r,b}, p_{r,t}, q_{3,t}, PP_{h,t}, \Delta T_{sat}, T_{ho}, \text{fluid}_b, \text{fluid}_t). \quad (12)$$

Following the thermodynamic analysis, the temperature profiles within each heat exchanger are evaluated to ensure that no heat exchange process violates the minimum pinch point imposed during the optimisation. This is particularly important for the intermediate heat-exchange process since the bottoming-cycle expander inlet condition is an output from the model. For this process, alongside the two pre-heating processes, the heat exchanger is discretised into 25 elements and the minimum temperature difference is determined.

Given the novelty of the system under investigation, and the lack of any suitable experimental data, a direct validation of the thermodynamic model is not currently possible. However, for the purpose of verification, the cascaded model has been modified to run with a specified bottoming-cycle mass-flow rate and specific input heat load, rather than specifying $PP_{h,t}$ and T_{ho} , enabling a comparison to a cascaded system previously studied within the literature [22]. The results reveal a relative difference in the mass-flow rates and thermal efficiencies that are less than 1% and 3.2% respectively, which are considered to be sufficiently small.

3.2. Expander modelling

To account for the effects of the cycle operating conditions on expander performance, expander models are implemented to estimate expander isentropic efficiency based on the volumetric expansion ratio. Here emphasis is placed on radial-inflow turbines and twin-screw expanders.

3.2.1. Radial-inflow turbine modelling

For applications below a few hundred kilowatts radial-inflow turbines are commonly employed. Broadly speaking, their efficiency depends on the volumetric expansion ratio, and the turbine size. The latter depends on the power rating of the system. The former is an effect of the thermodynamic cycle conditions, with high volumetric expansion ratios resulting in a reduced turbine efficiency.

Perdichizzi and Lozza [23] mapped radial-inflow turbine efficiency as a function of the isentropic volumetric expansion ratio ($V_{r,s} = \rho_3/\rho_{4s}$, where ρ_{4s} is the density following an isentropic expansion) and the size parameter ($SP = \dot{V}_{4s}^{1/2}/\Delta h_s^{1/4}$, where \dot{V}_{4s} is the outlet volumetric-flow rate following an isentropic expansion and Δh_s is the turbine isentropic enthalpy drop). More recently, a

similar map has been obtained using mean-line methods [24]. Previously, these maps have been used to develop a model that estimates isentropic efficiency η based on \dot{m} , $V_{r,s}$ and Δh_s [25]. This previous model considers the effects of $V_{r,s}$ on η , in addition to scaling effects. However, as the intention here is to compare radial-inflow turbines and twin-screw expanders, and simple methods to account for scaling effects in twin-screw expanders are not currently available, scaling effects within radial-inflow turbines will not be considered. Instead, the following simplified model is employed:

$$\frac{\eta}{\eta_{max}} = -0.004615V_{r,s} + 1.007, \quad (13)$$

where η_{max} is the maximum achievable efficiency.

3.2.2. Twin-screw expander modelling

Twin-screw expanders are generally used in applications with smaller volumetric expansion ratios than radial-inflow turbines, since they are limited by their built-in volume ratio, but can be used for two-phase expansion. The authors have previously developed a model to account for the effect of the volumetric expansion ratio on twin-screw expander efficiency [26], which is described here.

When sizing a twin-screw expander the parameters of primary interest are the volumetric expansion ratio ($V_r = \rho_3/\rho_4$), and the built-in volume ratio V_{bi} , which is the ratio of the maximum chamber volume to the volume at the point where the inlet port closes. This is determined by the shape of the opening in the casing of the machine, and is fixed for a given machine. Previously, Read et al. [27] found that expander efficiency is related to the ratio of these volume ratios, $R_{exp} = V_{bi}/V_r$. The relationship identified is shown in Fig. 9, which has a maximum at $R_{exp,opt} \approx 0.65$. This curve was obtained from simulations for one twin-screw machine, although it is expected that for any given machine, the performance curve will be similar in that it will have a quadratic form with $R_{exp,opt} < 1$.

The maximum built-in volume ratio, $V_{bi,max}$, is limited by mechanical design constraints; as the required V_{bi} increases, the inlet port area reduces, leading to higher pressure losses during filling. The inlet volumetric flow per revolution is also reduced, leading to reductions in mass flow rate and power output. Finding the optimal built-in volume ratio that achieves the maximum specific power is essential to identify the optimum thermodynamic performance of cycles using screw expanders. For an assumed value for $V_{bi,max}$, the maximum volumetric expansion ratio that can be achieved, without resulting in a reduction in expander isentropic efficiency, is given by:

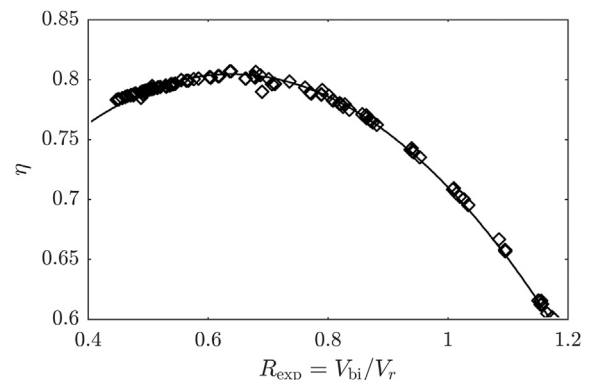


Fig. 9. Typical relationship between R_{exp} and the isentropic efficiency of a twin-screw expander [27].

$$V_{r,max} = \frac{V_{bi,max}}{R_{exp,opt}} \quad (14)$$

Thus, based on the quadratic performance curve and an assumed value for $V_{bi,max}$, an expression for the expander efficiency as a function of V_r can be derived. For $V_r \leq V_{bi,max}$ it is assumed that an expander can be selected that has an optimal built-in volume ratio such that $R_{exp} = R_{exp,opt}$. For $V_r > V_{bi,max}$, the expander isentropic efficiency can be estimated using the quadratic performance curve. This is expressed as follows:

$$\eta = \begin{cases} \eta_{max}, & \text{if } V_r \leq V_{r,max} \\ a_1 R_{exp}^2 + a_2 R_{exp} + a_3 & \text{otherwise,} \end{cases} \quad (15)$$

where $\eta_{max} = -a_2^2/4a_1 + a_3$ and $R_{exp} = V_{bi,max}/V_r$.

If $V_{bi,max} = 5$, which is a reasonable assumption for a twin-screw machine, and the performance curve shown in Fig. 9 is assumed, the maximum volumetric expansion ratio that can be achieved without a reduction in efficiency is $5/0.65 = 7.7$. The coefficients for the quadratic are $a_1 = -0.7205$, $a_2 = 0.9230$ and 0.5100 , and thus $\eta_{max} = 0.806$. The resulting curve is shown in Fig. 10.

3.3. Heat-exchanger sizing

3.3.1. Cross-flow evaporator

The heat exchanger that transfers heat from the heat source to the working fluid is assumed to be a finned-tube cross-flow evaporator (Fig. 11), which facilitates a large heat-transfer area on the exhaust-gas side, which has the largest thermal resistance. To account for fluid property variation and the distinct single- and two-phase regions, the heat exchanger is discretised. Each cell is a vertical slice through the heat exchanger, defined by the height H and width W of the frontal area, the number of tubes in the direction perpendicular to the flow N_H , and the number of columns within the cell $N_{L,i}$ (where $N_L = \sum_i N_{L,i}$). To initialise the model an estimate for the number of columns is required, $N_{L,0}$, which is found from a single calculation for each of the preheating, evaporation and superheating regions. The number of columns within each cell is $N_{L,i} = N_{L,0}/n$, where n is the target discretisation number. For each cell, the ϵ -NTU method for a mixed cross-flow heat exchanger is used to determine both outlet temperatures. This process is iterative since the heat-transfer coefficients for the working fluid,

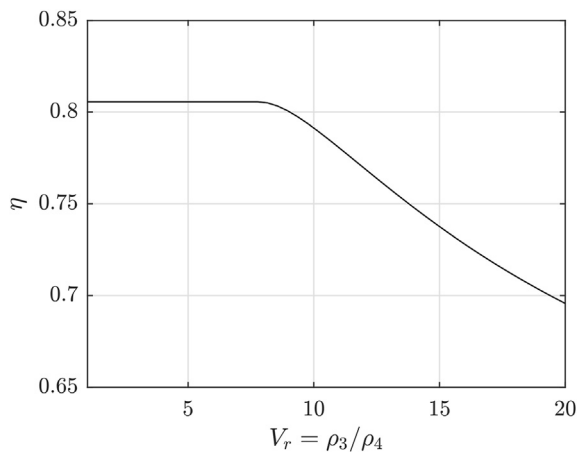


Fig. 10. Twin-screw expander efficiency as a function of V_r , assuming $V_{bi,max} = 5$, $a_1 = -0.7205$, $a_2 = 0.9230$ and 0.5100 .

α_w , and heat source, α_h , are calculated based on the mean properties. The overall calculation process employed is summarised within Fig. 12, and is similar to the process outlined in Ref. [28]. The correlations used for determining heat-transfer coefficients and friction factors are summarised in Table 1. It should be noted that the use of any heat-transfer correlation is likely to be subject to an error margin. However, in a comparative study such as this, where general trends are of more interest than the exact heat-exchanger sizes, their use can enable a quantitative comparison between different systems. Thus, whilst it is acknowledged that other correlations could be employed in place of those listed in Table 1, the primary consideration is that the same correlation is used consistently for the different heat-transfer processes.

To reduce computation time the assumptions listed in Table 2 are made which reduces the optimisation to one involving only the velocity of the incoming heat source V_h , and the pipe inner diameter D_i . Thus, these two variables can be optimised to minimise the heat-transfer area subject to imposed pressure drop constraints. For the cascaded systems, an integrated evaporator is proposed (Fig. 1). Thus, the inner pipe diameter for both the bottoming and topping cycle tubes are the same and the optimisation objective is to minimise the total combined area, subject to pressure drop constraints for the two working fluids, and a heat-source pressure drop constraint for the entire evaporator.

3.3.2. Double-pipe heat exchanger

Both the heat-rejection heat exchanger, and the intermediate heat exchanger that transfers heat between the topping- and bottoming-cycles, are assumed to be counter-flow double-pipe heat exchangers. Double-pipe heat exchangers are cost effective for small-scale applications, and since these processes predominantly involve either liquid or two-phase fluids, compact designs can be obtained. The heat-transfer areas are calculated using a discretised sizing methodology based on the log-mean temperature difference:

$$A = \sum_{i=1}^n \frac{\dot{Q}_i}{U_i \Delta T_{log,i}} \quad (16)$$

where n is the number of elements, and \dot{Q}_i , U_i and $\Delta T_{log,i}$ are the heat-transfer rate, overall heat-transfer coefficient and counter-flow log-mean temperature difference for the i^{th} element respectively. From the thermodynamic cycle analysis \dot{Q}_i and $T_{log,i}$ are known, and for assumed pipe diameters the heat-transfer coefficients, and hence U_i , can be readily found. It should be noted that in the case of the intermediate heat exchanger, where there is phase change on both sides of the heat exchanger, ΔT_{log} should be replaced with the difference in the saturation temperatures. The inner pipe is assumed to have the same wall thickness and thermal conductivity given in Table 2, whilst the optimisation variables are the pipe inner diameters. For the condenser the working fluid passes through the inner tube, whilst for the intermediate heat exchanger the high-pressure evaporating fluid passes through the inner tube. The correlations used for determining heat-transfer coefficients and friction factors are summarised in Table 1.

3.3.3. Pressure drop correction

Following heat-exchanger sizing the power outputs are corrected to account for heat-exchanger pressure drops. The pumps are assumed to operate over the pressure ratios defined by the cycle simulation, so the pressure drops lead to a reduction in the pressure change across the expander. Thus, the corrected expander inlet pressure is:

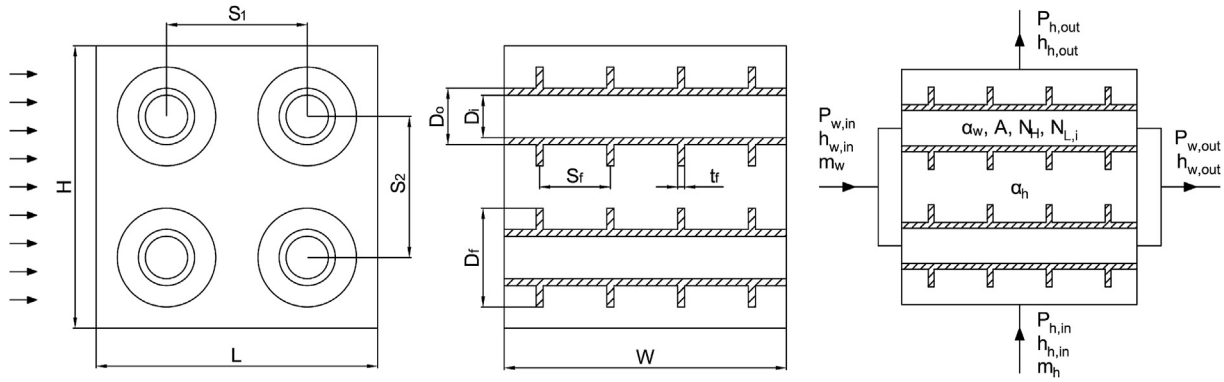


Fig. 11. Simplified schematic of the cross-flow evaporator. Left to right: side view; frontal view; description of a discretised cell.

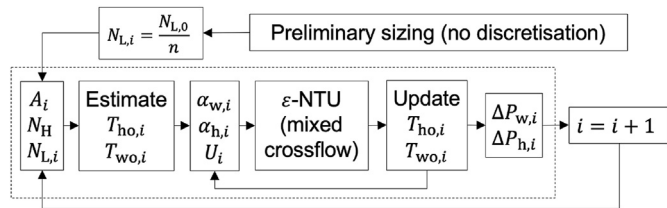


Fig. 12. Flow chart of the cross-flow evaporator sizing procedure.

$$p_3 = p_2 - \Delta p_{ph} - \Delta p_{ev} - \Delta p_{sh} , \quad (17)$$

where Δp_{ph} , Δp_{ev} and Δp_{sh} are the pressure drops within the pre-heating, evaporation and superheating regions. It is assumed that the pressure drops have a negligible effect on the temperature profiles within the heat exchangers, such that the heat-transfer rates, and thus expander inlet enthalpy, are unchanged from the initial cycle simulation and thus *i.e.*, $[\rho_3, T_3, s_3] = f(p_3, h_3)$. The corrected expander outlet pressure is:

$$p_4 = p_1 + \Delta p_{ds} + \Delta p_{co} , \quad (18)$$

where Δp_{ds} and Δp_{co} correspond to the pressure drops across the desuperheating and condensation regions respectively. Thus, from the recalculated expander inlet conditions and outlet pressure, the expansion process can be recalculated.

During the study described later, it is found that for cascaded systems the reduction in power resulting from the pressure drop correction is less than 1% for over 90% of the optimal systems that form the Pareto fronts identified during the multi-objective optimisation. For the single-stage systems, a larger drop in power is observed and this is less than 4% for over 80% of the optimal systems that form the Pareto front. However, the largest drops in power are observed at the middle of the Pareto front. At the point where power output is maximised, the reduction in power due to

the pressure drop correction was less than 1%. Therefore, neglecting pressure drops within the cycle analysis is not expected to have a significant effect on the results during a single-objective optimisation.

An alternative approach would be to couple the cycle and heat-exchanger models together. However, this would introduce the need to iterate between the cycle and heat exchanger models, which significantly increases calculation time, particularly when conducting multi-objective optimisation. The method described here is a compromise, but is still better than constraining the pressure drop to be below a certain percent and neglecting the effect of this pressure drop on the power output from the system.

3.4. Optimisation

A combination of single-objective optimisation (SOO) and multi-objective optimisation (MOO) studies are completed to identify optimal systems that maximise thermodynamic performance, and to investigate the trade-off between performance and heat-transfer area. Since the focus of this study is on waste-heat recovery applications, it is noted that power output is a better measure of thermodynamic performance than thermal efficiency and hence the optimisation can be formulated in the following general form:

$$\begin{aligned} & \min_{\mathbf{x}, \mathbf{y}} \{ -\dot{W}_n(\mathbf{x}, \mathbf{y}), A(\mathbf{x}, \mathbf{y}) \} \\ & \text{subject to :} \\ & g(\mathbf{x}, \mathbf{y}) \leq 0 \\ & h(\mathbf{x}, \mathbf{y}) \leq 0 \\ & \mathbf{x}_{\min} \leq \mathbf{x} \leq \mathbf{x}_{\max} \\ & \mathbf{y}_{\min} \leq \mathbf{y} \leq \mathbf{y}_{\max} \end{aligned} \quad (19)$$

where \mathbf{x} and \mathbf{y} define the cycle and the heat-exchanger design variables, $g(\mathbf{x}, \mathbf{y})$ and $h(\mathbf{x}, \mathbf{y})$ are the cycle and heat-exchanger constraints, and $\mathbf{x}_{\min} \leq \mathbf{x} \leq \mathbf{x}_{\max}$ and $\mathbf{y}_{\min} \leq \mathbf{y} \leq \mathbf{y}_{\max}$ are the bounds on the optimisation variables. Depending on whether a single-stage or cascaded cycle is considered, \mathbf{x} is defined by the

Table 1
Correlations used for heat-exchanger design.

Fluid	Phase	Nusselt number, Nu	Pressure drop
working fluid	single-phase	Dittus-Boelter [29]	Petukhov friction factor [30]
	evaporation	Chen [31]	Müller-Steinhagen and Heck [32]
	condensation	Shah [33]	Müller-Steinhagen and Heck [32]
air (heat source) ^a	single-phase	Schmidt [34]	Gaddis & Gnielinski [35]
water (heat sink)	single-phase	Dittus-Boelter [29]	Petukhov friction factor [30]

^a Correlations for cross-flow over a bank of finned tubes with an in-line arrangement.

Table 2
Fixed geometrical parameters for the cross-flow evaporator.

Parameter	Value	Comment
W/H	1.0	Frontal area is square, hence $W = H = \sqrt{\dot{m}_h/(\rho V)_h}$
S_1/D_o	2.0	Space between pipes is equal to pipe outer diameter
S_1/S_2	1.0	Tubes are equally spaced in both directions
D_f/S_1	0.9	A value < 1 ensures fins do not interfere with fins of adjacent tubes
t_w	2 mm	Tube wall thickness
k_w	16 W/(m K)	Wall thermal conductivity; stainless steel
t_f/t_w	0.5	Fin thickness is half the tube wall thickness
S_f/t_f	5.0	Ratio of fin spacing to fin thickness

cycle variables, as indicated in Eqs. (1) and (12) respectively. For a single-stage system \mathbf{y} is defined by:

$$\mathbf{y} = [V_h, D_{i,ev}, D_{i,co}, D_{h,o,co}], \quad (20)$$

and for a cascaded system:

$$\mathbf{y} = [V_h, D_{i,ev}, D_{i,int}, D_{h,o,int}, D_{i,co}, D_{h,o,co}], \quad (21)$$

where D_i and $D_{h,o}$ refer to the inner pipe diameter and outer pipe hydraulic diameter respectively, and the subscripts ‘ev’, ‘co’ and ‘int’ refer to the evaporator, condenser and intermediate heat exchangers respectively.

The SOO studies are completed using the sequential quadratic programming (SQP) algorithm, which is a gradient-based optimiser suitable for constrained non-linear problems. To help ensure a global optimum is identified each optimisation is completed from 10 different start points. For the MOO studies, an elitist genetic algorithm is used to generate the Pareto front. The algorithm is a variant of the non-dominated sorting genetic algorithm (NSGA-II), and within this study the population size is set to 200 and the optimisation is completed when the average spread change in the Pareto front spread is less than $1e^{-4}$. An adaptive mutation function is used which randomly generates mutations based on the last successful or unsuccessful generation, whilst the crossover functions takes a weighted average of the parents; the mutation and crossover fractions are set to 0.2 and 0.8 respectively. Both the genetic algorithm and SQP algorithm are available within the Global Optimisation Toolbox (MATLAB 2017a, The Mathworks, Inc.).

4. Case study definition

Three heat-source temperatures are considered, namely $T_{hi} = 473, 523$ and 573 K, whilst the heat source is assumed to be air with a mass-flow rate of 1 kg/s. The heat sink is assumed to be water at a temperature of 15 °C with a mass-flow rate of 1 kg/s, although an investigation considering this parameter is conducted later. The thermo-physical properties for both the heat source and heat sink are modelled using NIST REFPROP, and are found assuming an initial pressure of 1 bar. Moreover, considering that the specific-heat capacity of air varies between approximately 1.01 and 1.05 kJ/(kg K) for temperatures between 288 and 573 K, whilst the specific-heat capacity of water at 288 K is 4.2 kJ/(kg K), the ratio of heat-capacity rates is $(\dot{m}c_p)_c/(\dot{m}c_p)_h \approx 4.2$. The pumps are modelled assuming a fixed isentropic efficiency of 70%, whilst a minimum pinch-point temperature difference is set for the heat exchangers. For the SOO studies this is set to 10 K, whilst for the MOO studies this is relaxed to 2 K. The bounds for the optimisation parameters are summarised in Table 3.

Seven working fluids are considered (Table 3). For cascaded systems the number of optimisation studies required is proportional to the square of the number of fluids considered. Thus, other

optimal fluids may exist, but to evaluate all possible fluid combinations is unfeasible. However, the authors’ have previously demonstrated how heat-source temperature and critical temperature are linked for both single-stage [36] and cascaded systems [37], and these fluids have been selected as they are commonly considered and span a range of relevant critical temperatures. Nonetheless, future studies should investigate the effects of the fluid on the expansion process and optimisation results in more detail. For the single-stage systems, each working fluid is considered in turn, whilst for the cascaded systems every possible pairing is considered. As noted previously, each optimisation is completed from 10 different start points; therefore, for each heat-source temperature, 70 optimisations are completed for the single-stage systems and 490 optimisations are completed for the cascaded cycles. The optimal cycle is the one that produces the maximum power.

Considering the time required to complete a MOO, it is not possible to evaluate every possible fluid combination. Instead, the MOO is completed using the single working fluid, or working fluid pair, that results in the largest power output, as identified from the SOO study. This is appropriate since the authors previous work suggests that the optimum fluid is independent of whether the objective is to maximise power output or minimise heat-transfer area [25].

5. Results and discussion

Previously, the models described have been used to conduct a preliminary comparison of single-stage and cascaded systems for WHR applications [17,18]. The results from these previous simulations were summarised in Fig. 2, which show that cascaded cycles, with a twin-screw expander in the topping cycle and a turbine in

Table 3
Fixed assumptions, optimisation parameters and list of working fluids considered.

Fixed assumptions	value	units	Fluid	T_{cr} [K]		
Heat source	air	–	isobutane	407.8		
T_{hi}	473, 523, 573	K	R245fa	427.2		
\dot{m}_h	1	kg/s	R1233zd	438.8		
Heat sink	water	–	isopentane	460.4		
T_{ci}	288	K	n-pentane	469.7		
\dot{m}_c	1, 4	kg/s	cyclopentane	511.7		
p_h, p_c	100	kPa	benzene	562.0		
Variable	min.	max.	units	Other	value	units
$T_1, T_{1,b}$	298	373	K	η_p	70	%
$p_r, p_{r,b}, p_{r,t}$	0.05	0.85	–	PP_{min}	10 (SOO)	K
$q_3, q_{3,t}$	0 (screw)	2	–		2 (MOO)	K
	1 (turbine)	2	–			
$PP_h, PP_{h,t}, \Delta T_{sat}$	10 (SOO)	100	K			
	2 (MOO)	100	K			
T_{ho}	288	T_{hi}	K			
V_h	1	20	m/s			
$D_i, D_{h,o}$	0.001	1.0	m			

bottoming cycle (2-ST), can achieve an increase in performance, compared to a single-stage system operating with a turbine (1-T), and require the smallest increase in total heat-transfer area of the cascaded systems considered. Exergy analysis was also reported in this previous work, which indicated that exergy destruction within the combined expansion processes of the cascaded system is between 19% and 37% less than the equivalent single-stage systems, whilst the additional exergy destruction introduced during the intermediate heat-transfer process is relatively low, contributing to less than 6% of the total exergy destruction [18]. However, whilst exergy analysis remains a useful tool to assess internal reversibility, the primary concern for waste-heat recovery applications remains maximising power. Thus, the focus here will be on comparing 1-T and 2-ST systems in greater detail considering the primary performance metric of power output, whilst considering sizing aspects such as heat-transfer area.

The optimal working fluids and working-fluid pairs for the 1-T and 2-ST systems for the different heat-source and heat-sink conditions considered within this paper are summarised in Table 4. However, for the sake of brevity, only the key thermodynamic operating conditions are presented, which are discussed later in Section 5.4. Remaining information on the optimised cycle variables are provided in the supplementary material (see Appendix B).

5.1. Expander efficiency sensitivity studies

The first investigation considers the sensitivity of the results to the values selected for the expander models, namely $\eta_{t,max}$, a_1 , a_2 , a_3 and $V_{bi,max}$. For this, the cycle optimisation studies for the 1-T and 2-ST systems were repeated for a range of different values for these inputs, although, to reduce computational time, it is assumed that the optimal working fluids are unchanged from those initially identified.

The sensitivity of the optimisation results to $\eta_{t,max}$ are reported in Fig. 13, from which it is observed that a lower value leads to an improvement in the 2-ST cycles relative to the 1-T systems. This is not surprising, since the 1-T cycles are more reliant on the turbine efficiency than the 2-ST cycles. More importantly, it is observed that the conclusions previously made (see Fig. 2) still remain valid, namely that for the 523 and 573 K systems the 2-ST systems generate more power than the 1-T systems.

The performance curve reported in Fig. 10 was obtained for one twin-screw machine operating with a single fluid. However, any twin-screw expander should exhibit similar behaviour, with a peak efficiency at a particular volumetric expansion ratio, and a drop in efficiency as the volumetric expansion ratio is either increased and reduced, owing to over- and under-expansion losses respectively. Thus, a study has been conducted to consider the sensitivity of the results to a shift of this curve in either the x - or y -direction (Δx and Δy), or a shift in the distance between the roots of the quadratic curve ($\Delta(\Delta x_{root})$), as depicted in Fig. 14. The results also depend on

Table 4
Optimal working fluids for the different heat-source and heat-sink conditions for the single (1-T) and cascaded (2-ST) cycles; the labels (t) and (b) correspond to the topping and bottoming cycles respectively.

T_{hi} [K]	\dot{m}_c [kg/s]	working fluid		
		1-T	2-ST (t)	2-ST (b)
473	1	R245fa	<i>n</i> -pentane	isobutane
473	4	R245fa	cyclopentane	isobutane
523	1	<i>n</i> -pentane	benzene	isopentane
523	4	R1233zd	benzene	R1233zd
573	1	cyclopentane	benzene	cyclopentane
573	4	cyclopentane	benzene	<i>n</i> -pentane

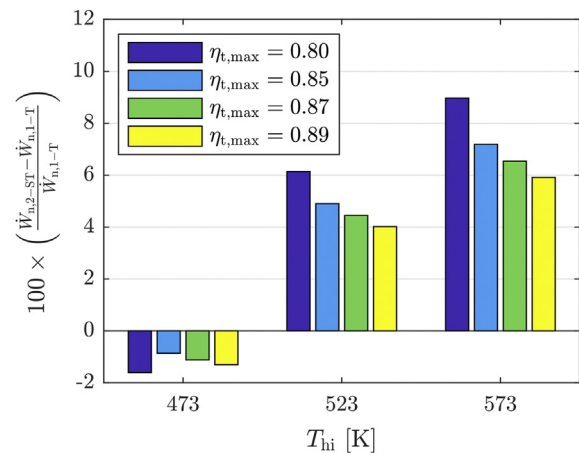


Fig. 13. Sensitivity of the single-objective optimisation results to the maximum value selected for the turbine efficiency, $\eta_{t,max}$. The results shown report the relative change in performance for a cascaded system (2-ST) compared to a single-stage (1-T) system. The screw performance curve is fixed to the one defined in Fig. 10.

$V_{bi,max}$. The effect of these four parameters on the performance curve is reported in Fig. 15, and the results from the sensitivity study are reported in Fig. 16.

The results appear most sensitive to a shift in the y -direction. More specifically, the change in the power output from the 2-ST system ranges between -4.4% and -1.9% for $\Delta y = -0.15$ and $+3.4\%$ and $+5.2\%$ for $\Delta y = +0.15$. By comparison, for the results for the Δx , $\Delta(\Delta x_{root})$ and $\Delta V_{bi,max}$ cases, with the exception of $\Delta V_{bi,max} = -3$, the change the power output is below $\pm 1\%$. It is worth noting that, because the twin-screw expander is in the topping cycle and the pressure ratio of the expander is relatively low, the volumetric expansion ratio across the expander is relatively low. Specifically, for the baseline 2-ST cycles the pressure ratios in the topping cycles for the 473, 523 and 573 K systems are 2.01, 2.97 and 3.51, whilst the volumetric expansion ratios are 4.27, 8.95 and 6.71 respectively. This implies that for all the cascaded systems a twin-screw expander can be selected that operates efficiently at the design point, and that the results are most sensitive to the assumed value for the peak efficiency, rather than the shape of the curve.

Thus, the two sensitivity studies suggest that the results are

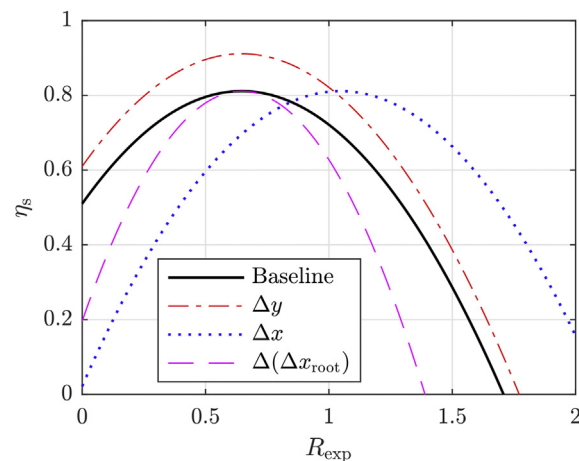


Fig. 14. Definitions used for the twin-screw expander sensitivity study: Δx and Δy refer to a shift in the x - and y -directions respectively, whilst $\Delta(\Delta x_{root})$ corresponds to a shift in the distance between the two roots to the quadratic performance curve.

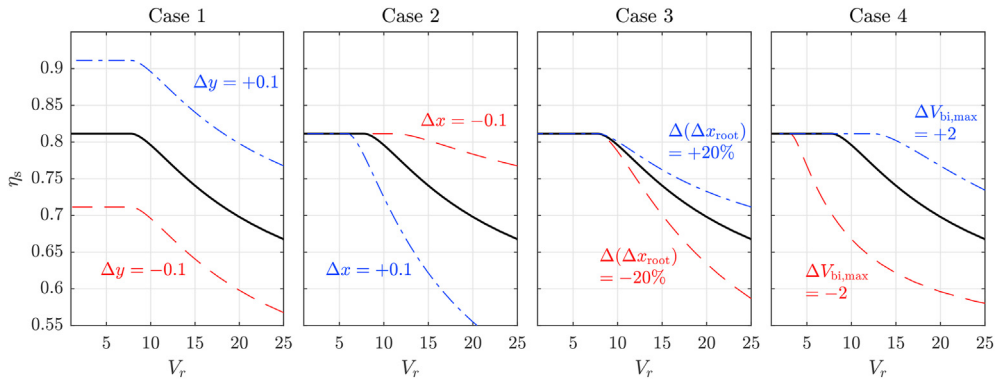


Fig. 15. Range of performance curves considered within the twin-screw efficiency sensitivity study.

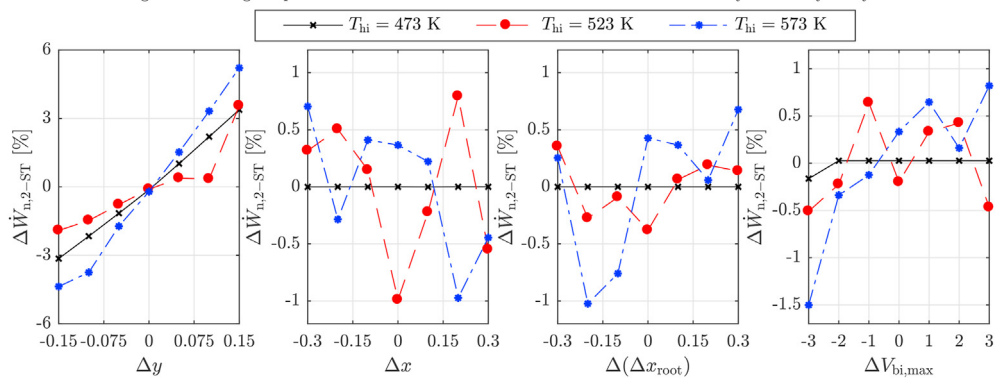


Fig. 16. Sensitivity of the SOO results to the screw performance curve with $\eta_{t,max} = 0.89$.

most sensitive to the two maximum expander efficiency values. However, the two efficiencies have been considered in isolation. The final study considers the sensitivity of the simulation to the two expander efficiencies simultaneously. The results from this study are reported in Fig. 17. These results show that for the 523 and 573 K heat-source temperatures, the 2-ST systems perform better than 1-T systems even in the least favourable condition (*i.e.*, $\eta_{t,max} = 0.89$ and $\eta_{s,max} = 0.65$). At this condition the 2-ST systems produce 4.3% and 2.4% more power than the 1-T systems for the 523 and 523 K systems respectively.

The results reported in Fig. 17 also provide a preliminary estimate on the effect of scale on the performance of cascaded systems. The expander performance curves are size independent since efficiencies are estimated from volumetric expansion ratios. However, it can be assumed that large-scale systems will correspond to higher efficiencies for both expanders, whilst small-scale systems

will correspond to lower efficiencies. The original study (Fig. 2) was based on values of $\eta_{t,max} = 0.89$ and $\eta_{s,max} = 0.80$ and it was found that the 2-ST systems produced 4.0% and 5.9% more power for the 523 and 573 K systems respectively. Reducing these to $\eta_{t,max} = 0.85$ and $\eta_{s,max} = 0.75$, which may be more reasonable for a small-scale system, the corresponding performance improvements are similar, corresponding to 5.6% and 6.3% respectively.

5.2. MOO results for $(\dot{m}c_p)_c/(\dot{m}c_p)_h \approx 4.2$

The results thus far reinforce the argument that for high heat-source temperatures a cascaded 2-ST system can outperform a single-stage 1-T system. However, this conclusion has been based only on the SOO studies, with no consideration of the required heat exchangers. Thus, for the 1-T and 2-ST systems, the MOO has been completed and the resulting Pareto fronts are reported in Fig. 18.

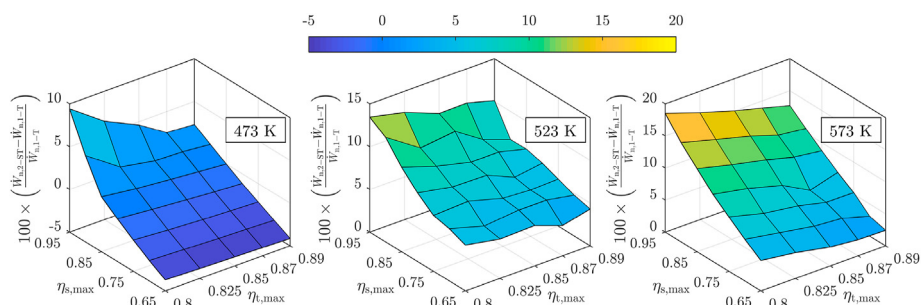


Fig. 17. Sensitivity of the SOO results to $\eta_{t,max}$ and $\eta_{s,max}$.

For these studies, the minimum allowable pinch-point constraint is relaxed to 2 K, and thus higher powers are obtained than previously identified from the SOO studies.

From these Pareto fronts, it is observed that at low power outputs (below 30 and 40 kW for the 523 and 573 K cases respectively), the single-stage systems produce the same amount of power as the cascaded systems, but require smaller heat exchangers. Thus, single-stage systems remain the best choice for applications where maximising the power output may not be the primary objective. However, for applications where maximising power output is the main objective, cascaded systems represent a more promising option. More specifically, from analysing the minimum pinch points for the optimal cycles on the Pareto fronts, it is observed that at high power outputs, the pinch points within the cascade systems tend to be larger than those within the single-stage systems. In other words, in the single-stage systems a point is reached where a further reduction to the pinch point results in a significant increase in the required area (i.e., as $PP_{\min} \rightarrow 0$, $A \rightarrow \infty$). However, since the pinch points in the cascaded system for the same power output are larger, these can be further reduced to increase the power output, with a less significant increase in heat-transfer area. Comparing the 523 and 573 K systems, the relative performance improvement between the single and cascaded systems increases as the heat-source temperature increases. This reaffirms the previous conclusion that cascaded cycles are a better choice for higher temperature heat sources. Taking as a reference case a total heat-transfer area of $A_t = 400 \text{ m}^2$, it is found that for this fixed heat-transfer area the 2-ST systems produce approximately 3.6% and 10.5% more power than the 1-T systems for the 523 and 573 K cases respectively.

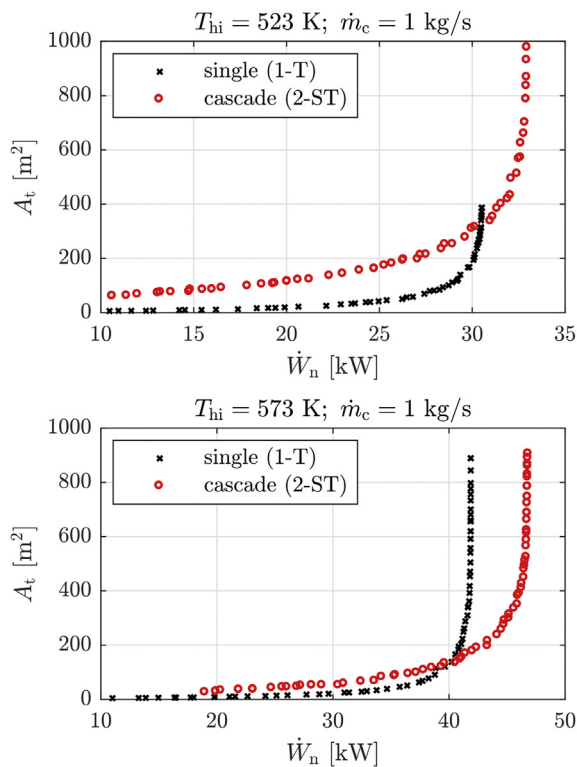


Fig. 18. Pareto fronts obtained from the multi-objective optimisation for the 523 K (top) and 573 K (bottom) heat-source temperatures for a heat-sink mass-flow rate of 1 kg/s ($\eta_{t,\max} = 0.89$; $\eta_{s,\max} = 0.806$).

5.3. Results for $(\dot{m}c_p)_c/(\dot{m}c_p)_h \approx 16.8$

To investigate the effect of the heat-sink mass-flow rate, the SOO and MOO optimisations have been repeated, increasing \dot{m}_c from 1 to 4 kg/s, which thus increases the ratio of heat-capacity rates from approximately 4.2 to 16.8. All other assumptions remain the same.

For brevity, the results from the SOO study are provided in the supplementary material (see B). However, it is noted that, for larger heat sinks, there is an increase in the relative performance improvement of 2-ST systems compared to 1-T systems. For the 473, 523, and 573 K cases, the 2-ST systems produce 7.5%, 11.1% and 12.4% more power than the equivalent 1-T systems. This is compared to values of -1.3% , 4.0% , and 5.9% previously obtained for $\alpha = 4.2$. This is because increasing \dot{m}_c results in smaller heat-sink temperature increases, which lowers the condensation pressure in the bottoming cycle of a 2-ST system. This reduces the bottoming cycle evaporation pressure to limit the volumetric expansion ratio across the turbine and thus maintain a high turbine efficiency. This, in turn, increases the pressure ratio in the topping cycle. In the 1-T systems, it is also possible to reduce the condensation temperature, but this increases the volumetric expansion ratio across the turbine, leading to a reduction in turbine efficiency, and a drop in performance. As an example, consider the results for the 473 K case, where the volumetric expansion ratio for the 1-T system increases from 13.3 to 18.6 when increasing \dot{m}_c from 1 to 4 kg/s. In comparison, the volumetric expansion ratios in the bottoming and topping cycles increase from 4.3 to 6.7, and from 4.3 to 5.9, respectively. Ultimately, this suggests that as the relative size of the heat sink increases, the case for the 2-ST systems improves. Moreover, these results also suggest that 2-ST systems may be suitable for heat-source temperatures below 473 K, provided that the heat-sink is sufficiently large.

The Pareto fronts obtained from the MOO are reported in Fig. 19, from which the same trends identified in the previous section hold true. Specifically, at lower power outputs, single-stage systems produce the same power but require smaller heat exchangers. However, at larger power outputs, there is an advantage to using a cascaded system. Moreover, when comparing the results shown in Figs. 18 and 19, a larger relative performance increase for the cascaded systems is observed as α increases. The reason for this was outlined in the previous paragraph, and thus the MOO results reaffirm the conclusion that cascaded systems perform better as α increases. Taking the same reference case as before, namely a total heat-transfer area of $A_t = 400 \text{ m}^2$, it is found that for this fixed heat-transfer area the 2-ST systems produce approximately 11.7% and 14.6% more power than the 1-T systems for the 523 and 573 K cases respectively. Thus, the cascaded produce more power whilst requiring the same heat-transfer area.

5.4. Thermodynamic comparison from a first- and second-law perspective

Whilst power output has been the primary focus of the present study, it is also useful to compare the 1-T and 2-ST in terms of the thermal efficiency of the cycle. For this purpose, the first-law thermal efficiency is introduced:

$$\eta_1 = \frac{\dot{W}_n}{\dot{Q}_h}; \quad (22)$$

alongside the second-law efficiency:

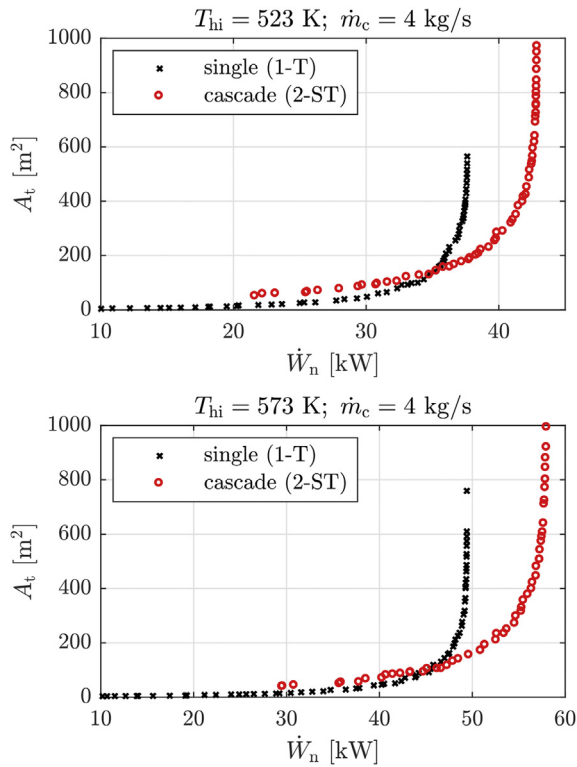


Fig. 19. Pareto fronts obtained from the multi-objective optimisation for the 523 K (top) and 573 K (bottom) heat-source temperatures for a heat-sink mass-flow rate of 4 kg/s ($\eta_{t,max} = 0.89$; $\eta_{s,max} = 0.806$).

$$\eta_{II} = \frac{\dot{W}_n}{\dot{E}_h}, \quad (23)$$

where \dot{Q}_h is the extracted from the heat source by the cycle, and \dot{E}_h is the exergy contained within the heat source. The latter is defined as:

$$\dot{E}_h = \dot{m}_h [(h_{hi} - h_{0,h}) - T_0 (s_{hi} - s_{0,h})], \quad (24)$$

where h_{hi} and s_{hi} are the enthalpy and entropy of the heat-source evaluated at the inlet conditions, T_0 is the dead-state temperature and $h_{0,h}$ and $s_{0,h}$ are the enthalpy and entropy of the heat-source fluid evaluated at the dead state, defined by $T_0 = 288$ K and a pressure of 101 kPa.

The power outputs, alongside η_I and η_{II} , for the optimised cycles for the different heat-source temperatures and heat-sink mass-flow rates are summarised in Table 5. The key cycle parameters for these cycles are also provided in Table 6. Ultimately, it is observed that for

Table 5

Thermodynamic performance of the optimised thermodynamic cycles obtained from the single-objective optimisation; the labels (t) and (b) correspond to the topping and bottoming cycles respectively.

T_{hi} [K]	\dot{m}_c [kg/s]	\dot{W}_n [kW]		η_I [%]		η_{II} [%]	
		1-T	2-ST	1-T	2-ST	1-T	2-ST
473	1	17.44	17.22	13.42	12.50	40.77	40.25
473	4	22.05	23.71	14.80	15.10	51.55	55.42
523	1	27.31	28.40	14.98	15.85	42.36	44.06
523	4	33.91	37.69	16.47	18.11	52.61	58.46
573	1	38.17	40.43	17.16	19.38	42.84	45.37
573	4	46.27	52.02	18.30	20.04	51.92	58.38

all cases except for the $T_{hi} = 473$ K, $\dot{m}_c = 1$ kg/s case, the 2-ST cycles outperform the 1-T cycles in terms of \dot{W} , η_I and η_{II} , with first-law efficiencies ranging between 12.5% and 20.0% and second-law efficiencies ranging between 40.3% and 58.5%. In terms of benefits of the cascaded cycle, the relative changes in first-law efficiency when moving from a 1-T cycle to a 2-ST cycle for $\dot{m}_c = 1$ kg/s are -6.9%, 5.8% and 12.9% for 473, 523 and 573 K heat-source temperatures respectively. Similarly, for $\dot{m}_c = 4$ kg/s the relative increases in η_I are 2.0%, 10.0%, and 9.5% respectively. Noting that for a defined heat-source, \dot{E}_h is constant and thus the relative improvements in η_{II} are the same as those already noted for \dot{W}_n ; namely -1.3%, 4.0% and 5.9% for $\dot{m}_c = 1$ kg/s and 5.1%, 11.1% and 12.4% for $\dot{m}_c = 4$ kg/s at the three heat-source temperatures. Ultimately, these results indicate that not only do the cascaded 2-ST cycles result in more power output than single-stage 1-T systems, but that the implementation of cascaded cycles also reduces internal irreversibility.

5.5. Preliminary economic consideration

A detailed economic comparison of the two systems is outside the scope of this study. However, as a preliminary assessment, the heat-transfer area required per unit power (i.e., A_t/\dot{W}_n) has been investigated across the Pareto front (Fig. 20). It is observed that single-stage systems are likely to be the cheapest option as they require the least amount of heat-transfer area to generate each unit of power. However, a system which requires a larger investment per unit power will generate more value over its lifespan. This trade-off requires further investigation.

6. Conclusions

This paper has investigated a novel cascaded ORC system (2-ST) for moderate-temperature waste-heat recovery applications (200–300 °C), which combines a two-phase expansion topping cycle through use of a twin-screw expander and a single-phase bottoming cycle operating with a radial-inflow turbine. This cycle could be a promising alternative to single-stage ORC systems employing a radial-inflow turbine (1-T). Thermodynamic cycle models have been integrated with variable efficiency expander models and heat-exchanger sizing models. This approach facilitates a single- and multi-objective optimisation of 1-T and 2-ST systems considering both thermodynamic and component performance, which enables a more rigorous comparison of the two systems than previously reported.

The results from the single-objective optimisations indicate that 2-ST systems could generate between 4.0% and 5.9% more power than 1-T systems for the 523 K and 573 K heat-source temperatures. For the 473 K case the optimal cascaded system generated 1.3% less power. After increasing the heat-sink mass-flow by a factor of four to represent an application with a larger available heat sink, the performance improvements for the 2-ST systems increased from -1.3%, 4.0% and 5.9%, to 7.5%, 11.1% and 12.4% respectively, indicating these systems may be best suited when the heat sink is sufficiently large. The results also reveal that the novel 2-ST cycle can increase first-law thermal efficiency by up to 9.5% compared to a single-stage 1-T system. A sensitivity study considering the expander efficiency models revealed that the results are most sensitive to the maximum values used for the expander efficiency curves, rather than the shape of the efficiency curves. For the analysed cases for the original heat sink size, reducing the maximum efficiencies for the radial-inflow turbine and twin-screw expander by 4% and 5% points respectively, resulted in the cascaded systems generating between 5.6% and 6.3% more power than the single-stage systems.

Table 6
Key cycle parameters for the optimised thermodynamic cycles obtained from the single-objective optimisation.

T_{hi} [K]	\dot{m}_c [kg/s]	T_3 [K]			p_3 [kPa]			p_2/p_1 [-]			\dot{m} [kg/s]		
		1-T	2-ST (t)	2-ST (b)	1-T	2-ST (t)	2-ST (b)	1-T	2-ST (t)	2-ST (b)	1-T	2-ST (t)	2-ST (b)
473	1	421.2	449.9	399.1	3103	2480	3085	9.38	2.01	4.31	0.569	0.314	0.380
473	4	408.8	450.0	393.7	2609	1850	2865	13.86	2.29	6.66	0.609	0.402	0.383
523	1	452.5	496.7	421.5	2480	2064	1817	14.06	2.97	7.81	0.347	0.458	0.381
523	4	446.6	489.8	407.6	3037	1862	2073	17.58	3.58	11.65	0.752	0.441	0.833
573	1	480.1	527.7	436.0	2717	3173	1467	18.57	3.51	10.13	0.396	0.410	0.392
573	4	442.9	510.7	396.7	1646	2519	973	26.11	6.14	9.84	0.448	0.385	0.490

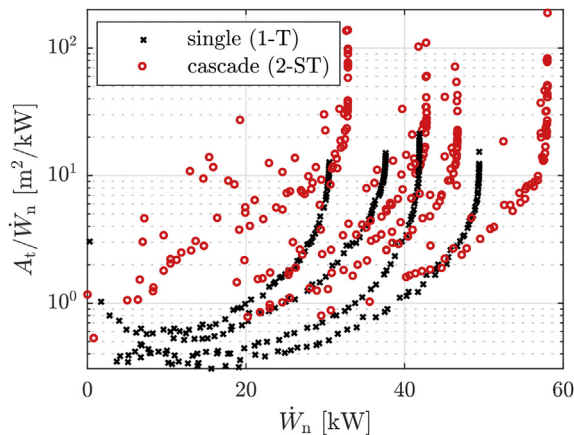


Fig. 20. Variation in heat-transfer area per unit power A_t/\dot{W}_n across the Pareto front for the single-stage and cascaded systems. The four groups of points for each system represent the different heat sources and heat sinks considered during the MOO studies.

The multi-objective optimisation studies reinforce that the novel 2-ST cycle can generate more power than the single-stage 1-T systems, but more interestingly indicate that despite requiring an additional heat exchanger, the increase in power is not necessarily associated with an increased heat-transfer area. Specifically, for a fixed total heat-transfer area of $A_t = 400 \text{ m}^2$, and $\dot{m}_c = 1 \text{ kg/s}$, the 2-ST systems produce approximately 3.6% and 10.5% more power than the 1-T systems for the 523 and 573 K cases respectively. This increases to 11.7% and 14.5% when \dot{m}_c is increased to 4 kg/s. Thus, for applications where maximising the power output may not be the primary objective, single-stage ORC systems remain the best option. However, in applications where the primary objective is to obtain the maximum power, cascaded systems can produce more power for the same amount of heat-transfer area. Thus, cascaded systems may be a promising candidate for high-performance applications. The next steps should be to conduct an economic assessment of the two systems, in addition to assessing off-design performance under both steady- and time-varying heat-source conditions.

Credit author statement

Martin White: Conceptualization, Methodology, Formal analysis, Writing - original draft; Matthew Read: Conceptualization, Writing - review & editing; Abdunaser Sayma: Writing - review & editing; Funding acquisition.

Declaration of competing interest

The authors declare that they have no known competing financial interests or personal relationships that could have appeared to influence the work reported in this paper.

Acknowledgements

This work was supported by the UK Engineering and Physical Sciences Research Council (EPSRC) [grant number: EP/P009131/1].

Appendix B. Supplementary data

Supplementary data to this article can be found online at <https://doi.org/10.1016/j.energy.2020.118912>.

Appendix A. Finite-time thermodynamics

Appendix A.1. General model for a heat engine

For a heat engine utilising a sensible heat source the power produced for a given change in the heat-source temperature is given by:

$$\dot{W} = \int \eta d\dot{Q}_h = (\dot{m}c_p)_h \int_{T_{h2}}^{T_{h1}} \eta dT_h, \quad (\text{A.1})$$

where \dot{m}_h and $c_{p,h}$ are the heat-source mass-flow rate and specific-heat capacity, η is the thermal efficiency, and T_{h1} and T_{h2} are the heat-source inlet and outlet temperatures. Using the Carnot efficiency ($\eta = 1 - T_c/T_h$) in Equation A.1 implies infinite heat-exchange processes that cannot be achieved in practice. Instead the efficiency that corresponds to the maximum work output from the cycle is applied [19, 20]:

$$\eta = 1 - \sqrt{\frac{T_c}{T_h}}. \quad (\text{A.2})$$

where T_c and T_h are the heat-sink and heat-source temperatures respectively. The change in the heat-source and heat-sink temperatures are related through:

$$dT_c = \left(\frac{1 - \eta}{\alpha} \right) dT_h, \quad (\text{A.3})$$

where α is the heat-capacity ratio, $(\dot{m}c_p)_c/(\dot{m}c_p)_h$. The solution to Equations A.1–A.3 results in an estimate for \dot{W} , based on T_{h1} , T_{h2} , the heat-sink inlet temperature T_{c1} , and α . The optimal value for T_{h2} that results in the maximum power can be found numerically.

Appendix A.2. Model for an isothermal heat sink

For an isothermal heat sink there is no change in heat-sink temperature, and the maximum power is produced when the heat source is cooled down to the heat-sink temperature. The solution of Equations A.1 and A.2 leads to:

$$\dot{W} = (\dot{m}c_p)_h \left[(T_{h1} - T_{c1}) - 2\sqrt{T_{c1}} \left(\sqrt{T_{h1}} - \sqrt{T_{c1}} \right) \right], \quad (\text{A.4})$$

where T_{h1} and T_{c1} denote the heat-source inlet and heat-sink temperatures. The heat rejected to the heat sink is:

$$\dot{Q}_c = \dot{Q}_h - \dot{W} = (\dot{m}c_p)_h (T_{h1} - T_{c1}) - \dot{W}. \quad (\text{A.5})$$

Appendix A.3. Model for an isothermal heat source

For an isothermal heat source there is no change in the heat-source temperature and the power output is given by:

$$\dot{W} = (\dot{m}c_p)_c \int_{T_{c2}}^{T_{c1}} \left(\frac{\eta}{1-\eta} \right) dT_c, \quad (\text{A.6})$$

where $(\dot{m}c_p)_c$ is heat-sink heat capacity rate, η is defined by Equation A.2, and T_{c1} and T_{c2} represent the heat-sink inlet and outlet temperatures respectively. Integrating this equation, and assuming the heat engine extracts a certain amount of heat from the latent-heat heat source, \dot{Q}_h , which is at a constant temperature T_h , the heat-sink outlet temperature is given by:

$$T_{c2} = \left(\frac{\dot{Q}_h}{2\sqrt{T_h}(\dot{m}c_p)_c} + \sqrt{T_{c1}} \right)^2. \quad (\text{A.7})$$

The heat rejected to the heat sink, $\dot{Q}_c = (\dot{m}c_p)_c (T_{c2} - T_{c1})$, and power output, $\dot{W} = \dot{Q}_h - \dot{Q}_c$, can then be obtained.

References

- Tartière T, Astolfi M. A world overview of the organic Rankine cycle market. *Energy Procedia* 2017;129:2–9. <https://doi.org/10.1016/j.egypro.2017.09.159>.
- Alshammari F, Pesyridis A, Karvountzis-Kontakiotis A, Franchetti B, Pasmazoglou Y. Experimental study of a small scale organic Rankine cycle waste heat recovery system for a heavy duty diesel engine with focus on the radial inflow turbine expander performance. *Appl Energy* 2018;215(October 2017):543–55. <https://doi.org/10.1016/j.apenergy.2018.01.049>.
- De Servi CM, Burigana M, Pini M, Colonna P. Design method and performance prediction for radial-inflow turbines of high-temperature mini-organic Rankine cycle power systems. *J Eng Gas Turbines Power* 2019;141(9):091021. <https://doi.org/10.1115/1.4043973>.
- Costall AW, Gonzalez Hernandez A, Newton PJ, Martinez-Botas RF. Design methodology for radial turbo expanders in mobile organic Rankine cycle applications. *Appl Energy* 2015;157:729–43. <https://doi.org/10.1016/j.apenergy.2015.02.072>.
- Read MG, Smith IK, Stosic N. Optimisation of power generation cycles using saturated liquid expansion to maximise heat recovery. *P I Mech Eng E-J Pro* 2017;23(1):57–69. <https://doi.org/10.1177/0954408916679202>.
- Smith IK. Development of the trilateral flash cycle system: Part 1: fundamental considerations. *P I Mech Eng A-J Pow* 1993;207(3):179–94. https://doi.org/10.1243/PIME_PROC_1993_207_032_02.
- Fischer J. Comparison of trilateral cycles and organic Rankine cycles. *Energy* 2011;36(10):6208–19. <https://doi.org/10.1016/j.energy.2011.07.041>.
- Kane M, Larrain D, Favrat D, Allani Y. Small hybrid solar power system. *Energy* 2003;28(14):1427–43. [https://doi.org/10.1016/S0360-5442\(03\)00127-0](https://doi.org/10.1016/S0360-5442(03)00127-0).
- Delgado-Torres AM, García-Rodríguez L. Double cascade organic Rankine cycle for solar-driven reverse osmosis desalination. *Desalination* 2007;216(1–3):306–13. <https://doi.org/10.1016/j.desal.2006.12.017>.
- Kosmadakis G, Manolakos D, Kyritsis S, Papadakis G. Economic assessment of a two-stage solar organic Rankine cycle for reverse osmosis desalination. *Renew Energy* 2009;34(6):1579–86. <https://doi.org/10.1016/j.renene.2008.11.007>.
- Rech S, Zandarin S, Lazzaretto A, Frangopoulos CA. Design and off-design models of single and two-stage ORC systems on board a LNG carrier for the search of the optimal performance and control strategy. *Appl Energy* 2017;204:221–41. <https://doi.org/10.1016/j.apenergy.2017.06.103>.
- Braimakis K, Karellas S. Exergetic optimization of double stage organic Rankine cycle (ORC). *Energy* 2018;149:296–313. <https://doi.org/10.1016/j.energy.2018.02.044>.
- Dubberke FH, Linnemann M, Abbas WK, Baumhögger E, Priebe KP, Roedder M, Neef M, Vrabec J. Experimental setup of a cascaded two-stage organic Rankine cycle. *Appl Therm Eng* 2018;131:958–64. <https://doi.org/10.1016/j.applthermaleng.2017.11.137>.
- Chen T, Zhuge W, Zhang Y, Zhang L. A novel cascade organic Rankine cycle (ORC) system for waste heat recovery of truck diesel engines. *Energy Convers Manag* 2017;138:210–23. <https://doi.org/10.1016/j.enconman.2017.01.056>.
- Manente G, Lazzaretto A, Bonamico E. Design guidelines for the choice between single and dual pressure layouts in organic Rankine cycle (ORC) systems. *Energy* 2017;123:413–31. <https://doi.org/10.1016/j.energy.2017.01.151>.
- Rashwan SS, Dincer I, Mohany A. Analysis and assessment of cascaded closed loop type organic Rankine cycle. *Energy Convers Manag* 2019;184(December 2018):416–26. <https://doi.org/10.1016/j.enconman.2018.12.089>.
- White M, Read M, Sayma A. Comparison between single and cascaded organic Rankine cycle systems accounting for the effects of expansion volume ratio on expander performance. In: 11th international conference on compressors and their systems; 2019. 9–11 September, London, UK.
- White MT, Read MG, Sayma AI. A comparison between cascaded and single-stage ORC systems taken from the component perspective. In: 5th international seminar on ORC power systems; 2019. p. 113. 9–11 September, Athens, Greece.
- Novikov II. The efficiency of atomic power stations (A review). *J Nucl Energy II* 1958;7(1–2):125–8. [https://doi.org/10.1016/0891-3919\(58\)90244-4](https://doi.org/10.1016/0891-3919(58)90244-4).
- Curzon FL, Ahlborn B. Efficiency of a Carnot engine at maximum power output. *Am J Phys* 1975;43(22):22–4. <https://doi.org/10.1119/1.10023>.
- White M. The design and analysis of radial inflow turbines implemented within low temperature organic Rankine cycles, Phd. City. University of London; 2015.
- Kosmadakis G, Manolakos D, Kyritsis S, Papadakis G. Design of a two stage Organic Rankine Cycle system for reverse osmosis desalination supplied from a steady thermal source. *Desalination* 2010;250(1):323–8. <https://doi.org/10.1016/j.desal.2009.09.050>.
- Perdichizzi A, Lozza G. Design criteria and efficiency prediction for radial inflow turbines. In: Gas turbine conference and exhibition; 1987. p. 87. GT–231.
- Lio LD, Manente G, Lazzaretto A. A mean-line model to predict the design efficiency of radial inflow turbines in organic Rankine cycle (ORC) systems. *Appl Energy* 2017;205(July):187–209. <https://doi.org/10.1016/j.apenergy.2017.07.120>.
- White MT, Sayma AI. Simultaneous cycle optimization and fluid selection for ORC systems accounting for the effect of the operating conditions on turbine efficiency. *Front Energy Res* 2019;7:50. <https://doi.org/10.3389/fenrg.2019.00050>.
- White MT, Read MG, Sayma AI. Using a cubic equation of state to identify optimal working fluids for an ORC operating with two-phase expansion using a twin-screw expander. In: 17th international refrigeration and air conditioning conference; 2018. p. 2172. 9–12 July, Purdue, U.S.
- Read M, Smith I, Stosic N. Effect of air temperature variation on the performance of wet vapour organic Rankine cycle systems. *Trans Geoth Resour Counc* 2014;38:705–12.
- Kaya A, Lazova M, Paeppe MD. Design and rating of an evaporator for waste heat recovery organic Rankine cycle using SES36. In: Proceedings of the 3rd international seminar on ORC power systems; 2015. p. 1–10. 12–14 October, Brussels, Belgium.
- Dittus FW, Boelter LM. Heat transfer in automobile radiators of the tubular type. *Int Commun Heat Mass Tran* 1985;12(1):3–22. [https://doi.org/10.1016/0735-1933\(85\)90003-X](https://doi.org/10.1016/0735-1933(85)90003-X).
- Petukhov B. Heat transfer and friction in turbulent pipe flow with variable physical properties. *Adv Heat Tran* 1970;6:503–64. [https://doi.org/10.1016/S0065-2717\(08\)70153-9](https://doi.org/10.1016/S0065-2717(08)70153-9).
- Chen JC. Correlation for boiling heat transfer to saturated fluids in convective flow. *Ind Eng Chem Proc DD* 1966;5(3):322–9.
- Muller-Steinhagen H, Heck K. A simple friction pressure drop correlation for two-phase flow in pipes. *Chem Eng Process* 1986;20(6):297–308. <https://doi.org/10.1175/BAMS-D-16-0178.1>.
- Shah MM. A general correlation for heat transfer during film condensation inside pipes. *Int J Heat Mass Tran* 1979;22(4):547–56. [https://doi.org/10.1016/0017-9310\(79\)90058-9](https://doi.org/10.1016/0017-9310(79)90058-9).
- Schmidt KG. M1 Heat transfer to finned tubes. In: VDI heat atlas. second ed. Springer-Verlag Berlin Heidelberg; 2010. p. 1273–7.
- Gaddis ES. L1.4 pressure drop of tube bundles in cross flow. In: VDI heat atlas. second ed. Springer-Verlag Berlin Heidelberg; 2010. p. 1076–91.
- White M, Sayma A. A generalised assessment of working fluids and radial turbines for non-recuperated subcritical organic Rankine cycles. *Energies* 2018;11(4):800. <https://doi.org/10.3390/en11040800>.

- [37] White M, Read M, Sayma A. Optimisation of cascaded organic Rankine cycle systems for high-temperature waste-heat recovery. In: 31st international conference on efficiency, cost, optimization, simulation and environmental impact of energy systems. Portugal: Guimarães; 2018. 17-22 June.

Nomenclature

Abbreviations

1-S: single-stage turbine
 1-T: single-stage turbine
 2-SS: cascaded system with two screw expanders
 2-ST: cascaded system with screw (bottom) and turbine (top)
 2-TS: cascaded system with turbine (top) and screw (bottom)
 2-TT: cascaded system with two turbines
 FTT: finite-time thermodynamics
 MOO: multi-objective optimisation
 ORC: organic Rankine cycle
 SOO: single-objective optimisation
 WHR: waste-heat recovery

Symbol

α : heat-capacity rate ratio
 α_h : heat-source heat-transfer coefficient, $W/(m^2 K)$
 α_w : working-fluid heat-transfer coefficient, $W/(m^2 K)$
 ΔT_{log} : log-mean temperature difference, K
 ΔT_{sat} : saturation temperature difference, K
 \dot{E} : exergy rate, J/s
 \dot{m} : mass-flow rate, kg/s
 \dot{Q} : heat-transfer rate, J/s
 \dot{V} : volumetric-flow rate, J/s
 W : power, J/s
 η : efficiency
 ρ : density, kg/m^3
 θ : non-dimensional heat-source temperature drop
 A : heat-transfer area, m^2
 c_p : specific-heat capacity at constant pressure, $J/(kg K)$
 D : tube diameter, m
 D_h : hydraulic diameter, m
 H : height of frontal area of cross-flow evaporator, m

h : specific enthalpy, J/kg
 L : length of cross-flow evaporator, m
 n : heat-exchanger discretisation number
 N_H : number of tubes along height of cross-flow evaporator
 N_L : number of tubes along length of cross-flow evaporator
 p : pressure, Pa
 p_r : reduced evaporation pressure
 PP : pinch point, K
 q : vapour quality
 S : cross-flow evaporator tube pitch, m
 s : specific entropy, $J/(kg K)$
 T : temperature, K
 t : thickness, m
 U : overall heat-transfer coefficient, $W/(m^2 K)$
 V_{bi} : built-in volume ratio
 V_r : volumetric expansion ratio
 W : width of frontal area of cross-flow evaporator, m

Subscripts

' : saturated conditions
 0 : dead state condition
 $1-4$: state points
 b : bottoming cycle
 c : heat sink
 co : condensing region
 cr : critical point
 ds : de-superheating region
 ev : evaporating region
 f : fin
 h : heat source
 I : first-law thermal efficiency
 i : inner, inlet
 II : second-law thermal efficiency
 int : intermediate
 max : maximum
 n : net
 o : outer, outlet
 p : pinch
 ph : preheating region
 s : conditions following isentropic expansion
 sh : superheating region
 t : topping cycle
 w : wall